AOARD Final Report

Grant FA2386-10-1-4115

Phenomenological studies of the response of granular and geological media to high-speed (Mach 1-5) projectiles

Koichi TANAKA
Primary Investigator
Department of Mechanical Engineering,
Chubu University,
1200 Matsumoto-cho, Kasugai-city 487-8501, Japan

Kazuyoshi TAKAYAMA
Co-primary Investigator
Shock Wave Interdisciplinary Application Division
Institute of Fluid Science, Tohoku University,
Katahira 2-1-1, Aoba-ku, Sendai 980-8577, Japan

Co-Investigtors

Keiko WATANABE
Department of Engineering Science, Osaka University,
Machikaneyama-cho 1-3, Toyonaka, Osaka 560-8531, Japan

Kiyonobu OHTANI
Shock Wave Interdisciplinary Application Division
Institute of Fluid Science, Tohoku University,
Katahira 2-1-1, Aoba-ku, Sendai 980-8577, Japan

Hiroaki YAMAMOTO
Shock Wave Interdisciplinary Application Division
Institute of Fluid Science, Tohoku University,
Katahira 2-1-1, Aoba-ku, Sendai 980-8577, Japan

Report Documentation Page

Form Approved
OMB No. 0704-0188

1. REPORT DATE	2. REPORT TYPE	3. DATES COVERED
06 OCT 2011	**Final**	**01-09-2010 to 31-08-2011**

4. TITLE AND SUBTITLE	5a. CONTRACT NUMBER
Phenomenological Studies of the Response of Granular and Geological Media to High-Speed (Mach 1-5) Projectiles II	**FA23861014115**
	5b. GRANT NUMBER
	5c. PROGRAM ELEMENT NUMBER
6. AUTHOR(S) **Koichi Tanaka**	5d. PROJECT NUMBER
	5e. TASK NUMBER
	5f. WORK UNIT NUMBER
7. PERFORMING ORGANIZATION NAME(S) AND ADDRESS(ES) **Chubu University,1200 Matsumoto-cho,Kasugai City 487-8501,Japan,NA,NA**	8. PERFORMING ORGANIZATION REPORT NUMBER **N/A**
9. SPONSORING/MONITORING AGENCY NAME(S) AND ADDRESS(ES) **AOARD, UNIT 45002, APO, AP, 96338-5002**	10. SPONSOR/MONITOR'S ACRONYM(S) **AOARD**
	11. SPONSOR/MONITOR'S REPORT NUMBER(S) **AOARD-104115**

12. DISTRIBUTION/AVAILABILITY STATEMENT
Approved for public release; distribution unlimited

13. SUPPLEMENTARY NOTES

14. ABSTRACT
This is the final report of the second year of a project to grasp various phenomena induced by the high-speed impact of projectiles on sand. These were the behavior of ejecta and the projectile, the penetration depth and speed of the projectile, and fractured grains and pressure distribution.

15. SUBJECT TERMS
Solid Mechanics, penetration mechanics, Shock Waves

16. SECURITY CLASSIFICATION OF:			17. LIMITATION OF ABSTRACT	18. NUMBER OF PAGES	19a. NAME OF RESPONSIBLE PERSON
a. REPORT	b. ABSTRACT	c. THIS PAGE			
unclassified	**unclassified**	**unclassified**	**Same as Report (SAR)**	**14**	

Abstract:

The objective of this research was to elucidate the response of geological media such as sand and soil to high-speed and high-pressure loading of projectiles. Particularly, penetration mechanics of high-speed projectiles into granular materials and response of granular media to shock waves were our substantial concern. One of unique the approaches we proposed was to collect numerical data and imaging data in laboratory scale experiments on high-speed projectile impacts using gun facilities and shock waves produced by micro-explosives in order to compare with large scale experiments. Another objective of this research was to establish tangible experimental methodology of data acquisition systems backed up with numerical data processing. In the first year scoping study, we focused ourselves on the fundamental test of several experimental methods for Eglin sand and Japan sand and successfully obtained several interesting experimental results. The present project followed along with the first year scoping studybut employed various developments in experimental methods.

Sand Behavior Induced by High-Speed Penetration of Projectile

Keiko Watanabe[*], Koichi Tanaka[**], Keisuke Iwane[*], Syungo Fukuma[*],
Kazuyoshi Takayama[***] and Hidetoshi Kobayashi[*]

[*] Department of Mechanical Science and Bioengineering, Osaka University,
1-3 Machikaneyama, Toyonaka, Osaka, 560-8531, Japan.
e-mail: keikow@me.es.osaka-u.ac.jp
[**] Department of Mechanical Engineering, Chubu University,
[***] Institute of Fluid Science, Tohoku University

Abstract: The primary objective is establishing tangible experimental methods and data analyzing methods in order to grasp various phenomena, which were the behavior of ejecta and projectile, the penetration depth and speed of projectile, fractured grains and the pressure distribution, induced by high-speed impact of projectile on sand. The plate impact experiments were conducted using vertical powder gun. The principal results are summarized as follows: Sands around the penetrated projectile were smashed to fine powder of 5 μm or less like a potato starch. Circumferential crashed sands were conically distributed and generated at impact velocity above 300 m/s. Conical massive crashed sand was produced ahead of projectile and vertical angle converged to around 60° as the velocity increases. The projectile penetrated at a speed about equal to the impact velocity in the initial penetration and decelerated rapidly over since.

1. INTRODUCTON

Collisions between geological materials and rigid bodies occur in various situations, which are excavation, construction, military application and asteroid impact. Accordingly, the impact and penetration of projectiles in soil have long been studied extensively[1-8]. However, for geological particulate materials such as sand, because the particle behavior is so complicated due to heterogeneity and instability of granular media, there have been few experiments investigating the impulse loading of these media, and the penetration properties on them are less understood. Dynamics of projectile penetration into sand depends greatly on the features of motion and state of the sand material at the interface with the projectile.

The final goal of this study is to develop an understanding of behavior of projectile during penetration, condition and distribution of comminuted sands and pressure distribution in sand under the impulse loading. As the first step, the primary objective is establishing tangible experimental methods and data analyzing methods in order to grasp various phenomena induced by high-speed impact of projectile on sand.

2. EXPERIMENT

Plate impact experiments were performed using vertical powder gun as shown in Fig.1. The projectiles with a mass of 12 or 12.5 g consisted of a plate impactor of stainless steel or brass 5 mm thick, 15 mm diameter, mounted on the front of a polycarbonate sabot as shown in Fig.2. The impact velocities investigated ranged from 150 to 1400 m/s.

The target was made up of quartz sands with a grain diameter of between 0.1 and 1 mm and a density of 2.65×10^3 kg/m^3. Grain size distribution was shown in Fig.3, and the grain size using in this experiment was 300~500 μm. The quartz sands were placed in three kinds of containers (see Fig.4 and Table 1). In the case of container B and C, the packing density was $1.49\sim1.56\times10^3$ kg/m^3, implying a porosity of 40~43 %.

Behavior of the ejecta and the projectile during initial penetration was visualized with high space and time resolutions using high-speed camera (MEMRECAM GX-8, NAC Image Technology Inc.) with 1,000 or 20,000 fps and ultra high-speed camera (ULTRA Cam HS-106E, NAC Image Technology Inc.) with 200,000 fps.

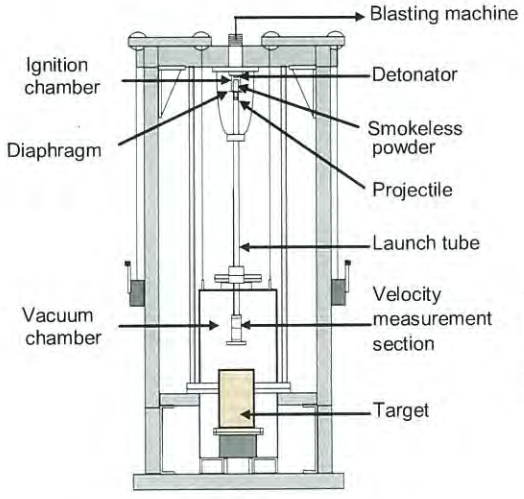

Fig.1 Vertical powder gun.

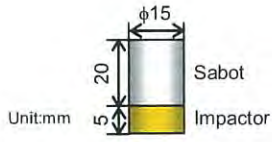

Fig.2 Projectile.

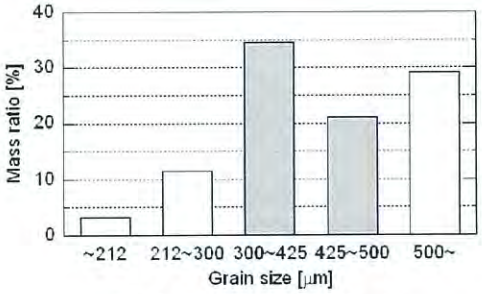

Fig.3 Grain size distribution.

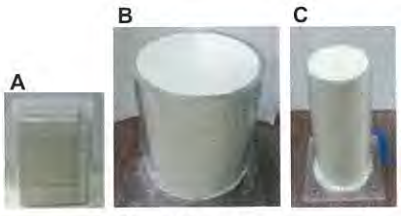

Fig.4 Container.

Table 1 Material and size of containers.

Container	A	B	C
Material	Polyethylene	PMMA	PMMA
Inner dia. [mm]	(115x155x155)	ϕ80	ϕ190
Thickness [mm]	1	5	10
Height [mm]	125	200	200

The two-dimensional pressure distribution of the depth direction was measured using the pressure sensitive films (Prescale, Fujifilm Co.) that were placed between the sand aggregate and the inner surface of an acrylic cylindrical container. When pressure is applied, the microcapsules are broken and the color-forming material reacts with the color-developing material. Red patches appear on the film and the color density changes according to the various pressure levels.

Optical glass fibers were used to detect optically the arrival time and trajectory of projectile in sand. The schematic illustration is shown in Fig. 5. The thin silica/silica fiber (core diameter; 200 μm, clad diameter; 220 μm) was selected and polyimide jacket was removed by sulfuric acid so that the penetration of projectile is prevented from disturbing. LED (L6112-01, Hamamatsu Photonics K.K.) and Si PIN photodiode (S5971, Hamamatsu Photonics K.K.) were used as light source and photo sensor, respectively. Beams of LED were passed through optical glass fibers which were arranged at 20 mm intervals, and photo sensors detect them. When the beam is blocked by cutting of fiber due to penetration of the projectile, the arrival time of projectile is detected.

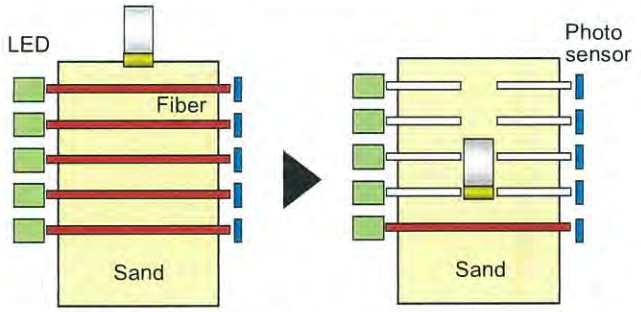

Fig.5 Schematic illustration of optical glass fiber detector.

3. RESULTS AND DISCUSSION

The investigation items to establish tangible experimental methods and data analyzing methods and results are summarized as follows:

3.1 High-Speed Visualization of Behavior of Ejecta and Projectile

Figure 6 shows continuous pictures of behavior of the ejecta from the surface of sand when the projectile penetrated into sand aggregate packed in container C at a speed of 350 m/s. Frame rate was 1,000 fps and exposure time was 50 μs. Sands were ejected radially like a crown and the velocity was about 20 m/s. It was found that the container wall greatly influenced the latter behavior of ejecta. Figure 7 shows continuous pictures of behavior of the projectile during initial penetration into sand aggregate packed in container C at a speed of 495 m/s. Frame rate was 20,000 fps and exposure time was 1 μs. Figure 8 shows detailed continuous pictures. Frame rate was 200,000 fps and exposure time was 300 ns. It was found that sands were at rest and the projectile penetrated at a speed about equal to the impact velocity in the initial penetration.

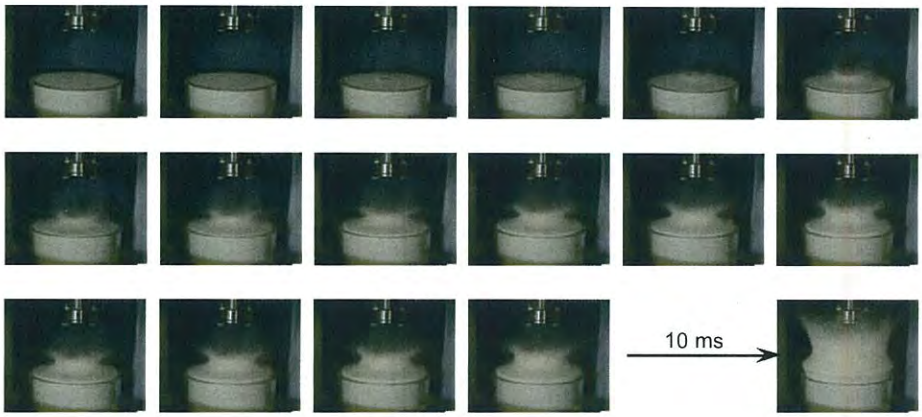

Fig.6 High-speed visualization of behavior of ejecta.
Frame rate; 1,000 fps, exposure time; 50 μs, impact velocity; 350 m/s, container; C.

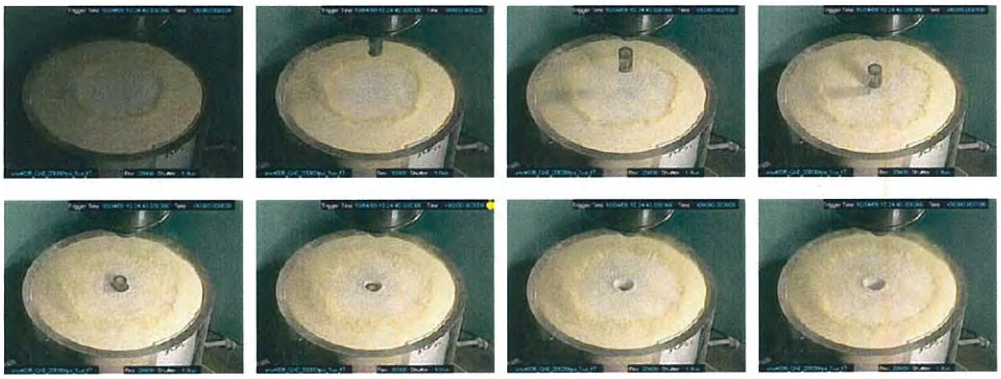

Fig.7 High-speed visualization of behavior of projectile during penetration.
Frame rate; 20,000 fps, exposure time; 1 μs, impact velocity; 495 m/s, container; C.

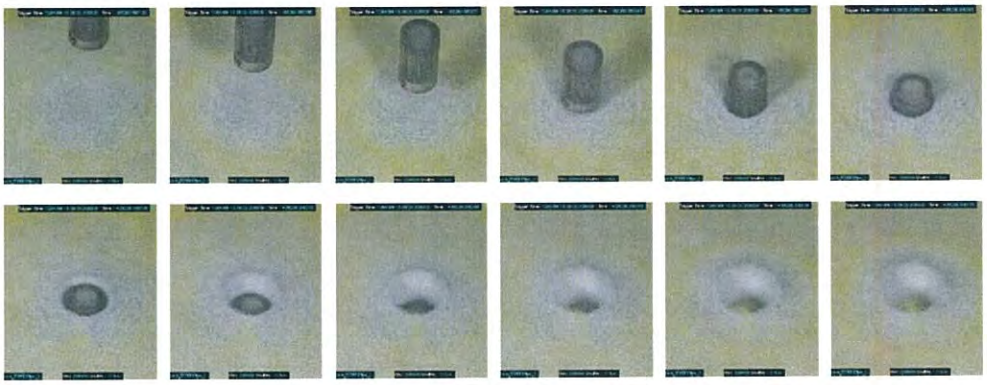

Fig.8 High-speed visualization of detailed behavior of projectile during penetration.
Frame rate; 200,000 fps (every 5 frames), exposure time; 300 ns,
impact velocity; 495 m/s, container; C.

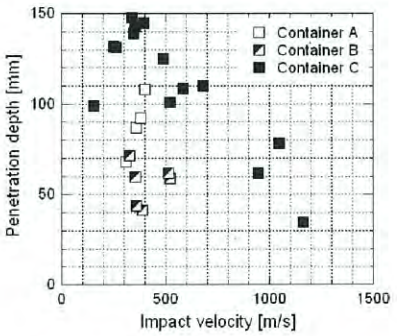

Fig.9 Effect of container type on relationship between impact velocity and penetration depth (impactor material; brass).

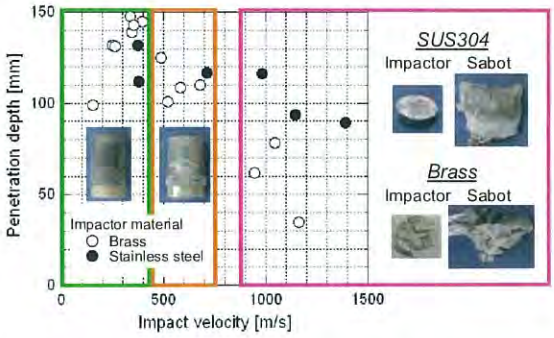

Fig.10 Effect of impactor material and deformation of projectile on relationship between impact velocity and penetration depth (container C).

3.2 Relationship between Impact Velocity and Penetration Depth

Figure 9 shows the effect of container type on the relationship between impact velocity and penetration depth. It was found that the relationship depended largely on the container types. In the case of container B, since the sand motion was strongly constrained by the container wall, the projectile didn't penetrate deeply and the container was broken to pieces over 600 m/s. Since container A made of polyethylene was easily deformed by applying a force, it was not fit to use. Figure 10 shows the effect of impactor material and deformation of projectile on the relationship between impact velocity and penetration depth. It was found that the degree of deformation of sabot and impactor greatly influenced the penetration depth. At a velocity below 450 m/s, the projectile did not change shape and the penetration depth increased with increasing the impact velocity. However, after 450 m/s, the projectile gradually began to deform and the penetration depth decreased with increasing the impact velocity. Especially, deformation of the brass impactor became large and the penetration depth was shallow in comparison with the stainless steel projectile.

3.3 Observation of Fractured Grains and Their Distribution

Sands around the penetrated projectile were smashed to fine powder of 5 μm or less like a potato starch as shown in Fig.11. It was found that there were two different kinds of distributions of crashed sands, which were circumferential and massive ahead of the projectile as shown in Fig.12. Circumferential crashed sands were powdery and generated at impact velocity above 300 m/s (see Fig.13). The distribution shape of circumferential crashed sands was an oblate cone (see the area inside thick line in Fig.14). On the other hand, the conical massive crashed sand was produced throughout all examined impact velocity range. Figure 15 shows the relationship between the vertical angle, 2α, of conical lump and the impact velocity. At a velocity below around 400 m/s, the vertical angle, 2α, decreased with increasing the impact velocity. However,

after around 400 m/s, the vertical angle, 2α, reached a constant when it reached about 60° and it did not increase any more even if the impact velocity increased. Figure 16 the relationship between the density of conical lump and the impact velocity. Upper line and lower line indicate the density of quartz (2.65×10^3 kg/m^3) and the original packing density ($1.49\sim1.56\times10^3$ kg/m^3), respectively. The density of conical lamp was approximately 2.0 to 2.6×10^3 kg/m^3 regardless of variations in the impact velocity, and it was found that the conical massive crashed sand was firmly pressed and compressed.

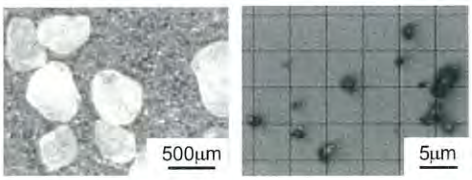

(a) Original sand (b) Crashed sand

Fig.11 Microscopic photographs of sand.

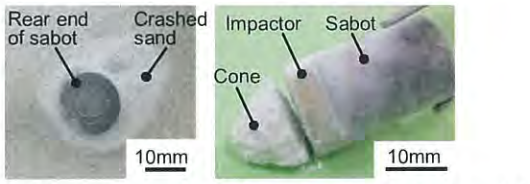

(a) Circumferential (b) Massive (ahead of projectile)

Fig.12 Distribution of crashed sand.

25168076825226342 4

(a) 250 m/s (b) 521 m/s.

Fig.13 Effect of impact velocity on generation of circumferential crashed sand.

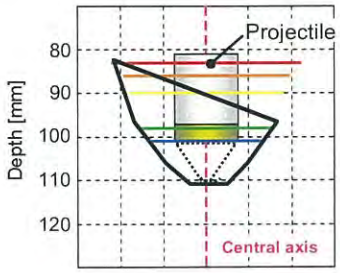

Fig.14 Measured cross-sectional distribution of crashed sand. Impact velocity; 521 m/s, penetration depth; 101 mm.

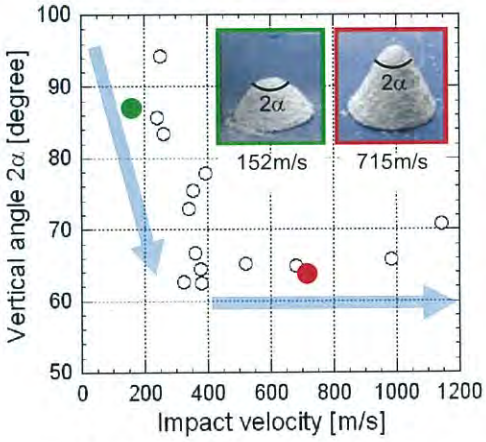

Fig.15 Effect of impact velocity on shape of massive crashed sand.

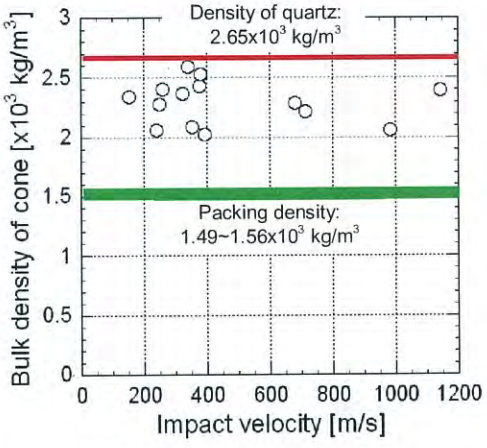

Fig.16 Effect of impact velocity on density of massive crashed sand.

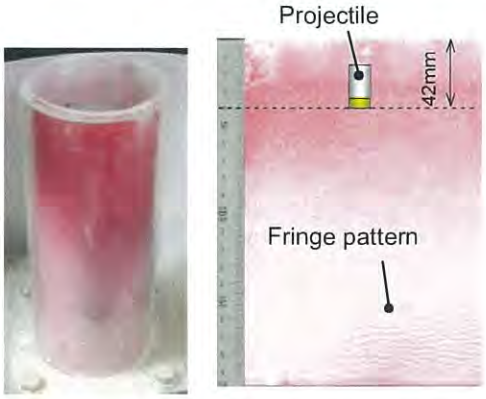

Fig.17 Two-dimensional pressure distribution on the inner wall of container B. Impact velocity; 389 m/s, penetration depth; 42 mm.

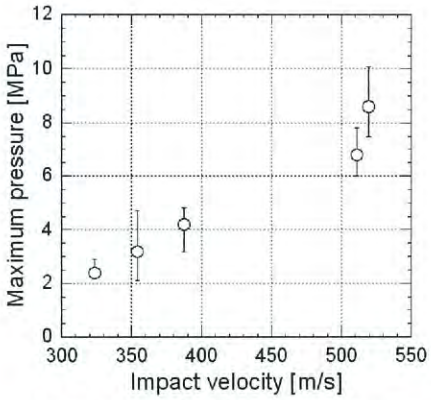

Fig.18 Relationship between maximum pressure and impact velocity (container B).

3.4 Measurement of Two-Dimensional Pressure Distribution

Figure 17 shows the actual pressure sensitive film in container B at a speed of 389 m/s. The penetration depth was 42 mm. The region between from the rear end of the stopped projectile to 30mm away from the stop position of projectile became darker color. At the lower part, a fringe pattern was produced due to interference of stress waves reflected from the container wall. Figure 18 shows the relationship between the maximum pressure and impact velocity. The Maximum pressure increased with increasing the impact velocity. It is theoretically predicted that container B is broken when the inner pressure exceeds about 10 MPa, and it was actually broken apart over 600 m/s as was stated previously in section 3.2. This indicates that this pressure measurement method is applicable to the quantitative analysis.

3.5 Detection of Behavior of Projectile during Penetration

Figure 19 shows the result obtained by optical glass fiber detector in container C at a speed of 250 m/s. The penetration depth was 144 mm. The projectile penetrated at a speed about equal to the impact velocity in the initial penetration and decelerated rapidly over since. This initial phenomenon was in agreement with the result obtained by high-speed photography as was stated previously in section 3.1.

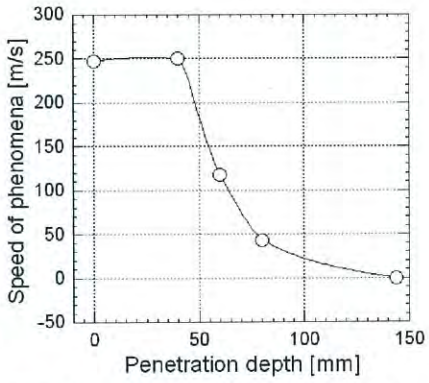

Fig.19 Example of result obtained by optical glass fiber detector. Impact velocity; 250 m/s, penetration depth; 144 mm.

4. SUMMARY AND CONCLUSION

In order to establish tangible experimental methods and data analyzing methods to grasp various phenomena induced by high-speed impact of projectile on sand, the plate impact experiments were conducted using vertical powder gun. The major results are summarized as follows:

1. Sands around the penetrated projectile were smashed to fine powder of 5 μm or less like a potato starch.
2. Circumferential crashed sands were conically distributed and generated at impact velocity above 300 m/s.
3. Conical massive crashed sand was produced ahead of projectile and vertical angle converged to around 60° as the velocity increases.
4. The projectile penetrated at a speed about equal to the impact velocity in the initial penetration and decelerated rapidly over since.

Acknowledgements

This research was supported by a research grant from The Mazda Foundation. The authors sincerely thank H. Sasaki and M. Shimawaki from NAC Image Technology Inc. for their excellent operation of the high-speed photography.

References

1. Allen, W.A., Mayfield, E.B., Morrison, H.L., Dynamics of a Projectile Penetrating Sand, *Journal of Applied Physics*, 1957, 28(3), 370-376.
2. Allen, W.A., Mayfield, E.B., Morrison, H.L., Dynamics of a Projectile Penetrating Sand. Part II, *Journal of Applied Physics*, 1957, 28(11), 1331-1335.
3. Lyubin, L.Y., Povitzkii, A.S., Oblique Impact of a Solid on Soils, *Journal of Applied Mechanics and Technical Physics*, 1966, 1, 55-60.
4. Savvateev, A.F., Budin, A.V., Kolikov, V.A., Rutberg, PH.G., High-Speed Penetration into Sand, *International Journal of Impact Engineering*, 2001, 26, 675-681.
5. Chen, X.W., Li, Q.M., Deep Penetration of a Non-Deformable Projectile with Different Geometrical Characteristics, *International Journal of Impact Engineering*, 2002, 27, 619-637.
6. Bragov, A.M, Lomunov, A.K., Sergeichev, I.V., Tsembelis, K, Proud, W.G., Determination of Physicomechanical Properties of Soft Soils from Medim to High Strain Rates, *International Journal of Impact Engineering*, 2008, 35, 967-976.
7. Brog, J.P., Volger, T.J., Mesoscale Simulations of a Dart Penetrating Sand, *International Journal of Impact Engineering*, 2008, 35, 1435-1440.
8. Sultanov, V.G., Kim, V.V., Lomonosov, I.V., Shutov, A.V., Fortov, V.E., Numerical Modeling of Deep Impact Experiment, *International Journal of Impact Engineering*, 2008, 35, 1816-1820.

An experimental study of penetration of a sphere into a sand layer

Hiroaki Yamamato, Brian Milton, Shokichi Hayasaka, Toshihiro Ogawa, Takamasa Kikuchi, Kiyonobu Ohtani, Kazuyoshi Takayama, William Cooper, Koichi Tanaka, Keiko Watanabe
Japan Association for the Advancement of Medical Equipment, 3-42-6 Hongo, Bunkyo-ku, Tokyo, 113-0033 JAPAN

Abstract

Paper reports the result of preliminary tests on determining penetration mechanics at hypersonic speed into particulate media. Using a vertical powder gun, we launched ϕ 9.53mm stainless spheres at speed ranging from 0.94 km/s to1.26 km/s into sand layers. In addition to dynamic pressure measurement in Eglin sand and glass beads, quantitative measurement was conducted to observe correlation between penetration depth, bulk density and impact velocity. To preserve impacted specimens, we used inorganic silicate-sealing agent and succeeded to freeze the trajectory of sphere's motion. Penetration velocity inside sand layer was measured by optical fiber breakdown velocity meter.

Key Words: high-speed penetration, sand layer, vertical powder gun, freezing technique

1. Introduction

The penetration mechanics of impacted particulate media involves destruction and abrasion etc. besides motion of particles. There are various experimental and theoretical studies on impacted particulate media [1]. However, compared to materials which have single phase, particulate media tend to be less characterized and consequently less understood, in particular, when subject to hypersonic impact.

Paper reports the result of preliminary tests to obtain quantitative information on the target/penetrator interaction.

2. Test Procedure

2-1 Test Materials

We used Florida coastal sand called Eglin Sand (Quikrete Commercial grade Fine Sand No.1961) and glass beads (Ballotini Glass Beads, size6, Batch SR 091208) for target material. Figure 1 shows micrograph of Eglin Sand. The particles of Eglin sand, largely consisting of Quartz, show slightly-angular shape. This is in contrast to the spherical shape of glass beads in Figure 1b. Figure 2 shows grain size distribution of Eglin Sand. It exhibits normal distribution of 361 μm of population mean and 0.733 of population variance.

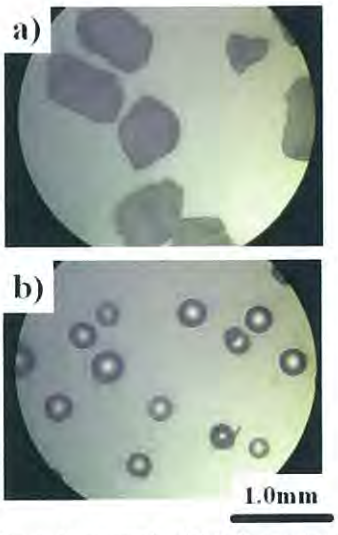

Fig. 1 Micrograph of a) Eglin sand and b) glass beads.

2-2 Ballistic range

The experimental projectile penetration data was obtained at Institute of Fluid Science, Tohoku University using a facility specifically converted for penetration type testing as shown in Figure 3.

In the present experiments, a series of 9.53 mm in diameter and 3.6 g weight, spherical stainless steel projectiles were fired vertically into a 150mm~ 300mm long 100mm diameter open top cylinder container or 200mm long by 100 mm by 30mm open top box. The test chamber was slowly filled with Eglin sand sieved to remove large debris and fine particles, using JIS standard sieve screen of 710μm and 355μm mesh. The bulk density of Eglin sand was controlled between 1.55 and 1.57 g/cm^3 by gently taped with a small rubber hammer.

3.0 grams smokeless gunpowder (HS-7) was put into cartridge case of rifle. A pneumatically-driven hammer was used for initiation. To increase velocity of projectile up to 1.26 km/s, extra smokeless powder (H50BMG) and black powder were set in the powder chamber. Sabot and projectile were set in the lower part of powder chamber. A plastic diaphragm was inserted between cartridge and sabot. The projectile was bonded at the tip of sabot. The sabot is frustum of a cone with flared end, made of super-high-molecular weight polyethylene (UHMWPE).

Sabot impinges on the stopper at the end of launcher tube, deformed sabot blocked nozzle and prevented the following combustion gas from blowing into the test chamber.

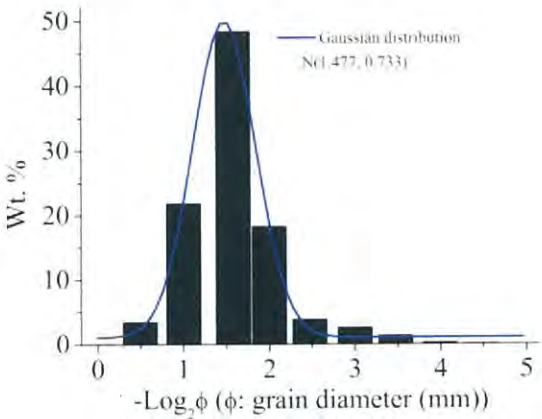

Fig. 2 Grain size distribution of Eglin sand.

The projectile separated from sabot flies in test chamber at the velocity from 0.97 km/s to 1.26 km/s.

The flight velocity was estimated by time difference between cutoff times of several linear laser beams placed at regular intervals by projectile.

2-3 Penetration velocity measurement

Figure 4 shows schematics of the velocity meter by the optical fiber breakdown. Five 0.2mm core diameter optical fibers (UV/VIS 200UM, NA=0.22, Edmund Optics) was arranged horizontally at regular intervals in the test chamber. The light source was a He-Ne laser (10 mW max. output at 632.0 nm, Melles Griot) coupled to 0.8mm core diameter optical fiber, which connects to a bundle of 0.2mm core diameter optical fibers inside test section. The detector was silicone PIN photodiodes (S5821, cutoff frequency: 25MHz, Hamamatsu photonics). The output signals were stored in a digital transient memory, Yokogawa-DL716 at sampling rate of 10MHz. Assuming that time of the optical fiber breakdown indicates transit time of projectile at the fiber position, the penetration velocity of projectile in sand layer was estimated.

2-4 Dynamic pressure measurement

When spherical stainless steel projectile plunges into sand layer, compression waves or shock waves are generated inside sand layer. These pressures were measured with pressure transducers, Kistler model 601B1 of rise time 2 μs, and resonant frequency of 300 kHz, flush mounted at the positions of A, B, C, D and E in Fig. 5. Pressure transducers were each accommodated in MC nylon adapters to avoid signals from electrical noise. The output signals from the pressure transducers transmitted to charge amplifiers, Kistler model 5011A and stored in a digital transient memory, Yokogawa-DL716 at sampling rate of 10MHz. To calibrate pressure transducers, we crosschecked the manufacturer's calibration chart by comparing it with pressure responses to known shock waves in air.

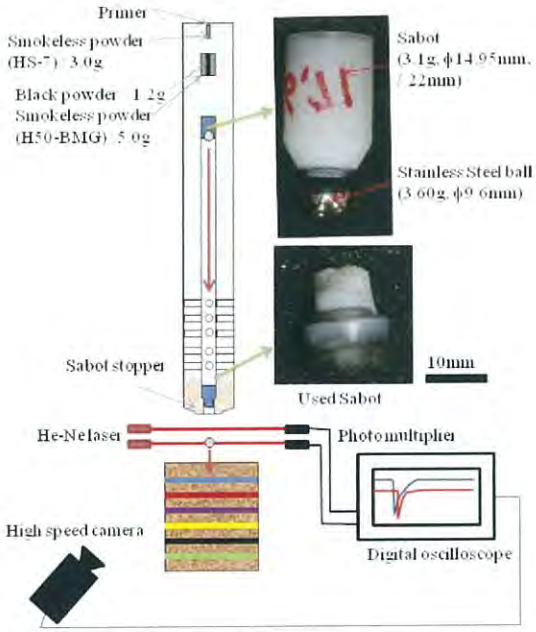

Fig. 3 Experimental setup for penetration test.

2-5. Freezing method of deformed sand layer

To observe the internal deformation of sand layer by penetration of projectile, colored maker layers were interlaminated in the sand layer. Sand particles have been stained with aqueous colored inks.

After firing, test chamber was retrieved and the whole specimens was dipped into a silicone-based inorganic polymer ('Permeate' D&D Corporation, Japan). This silicone sealer penetrates into the pores of sand layer without disturbance due to its low viscosity (15.5 mPa· s) and low surface tension (25.6 mN/m). After it interpenetrates into pores, it reacts with the moisture of ambient atmosphere and hardens due to the formation of inorganic polymer. After curing the sealant for a week, cross-sectional slices were created using circular saw machine. Then, we can readily estimate the track of the projectile and the accompanying deformation of sand layer.

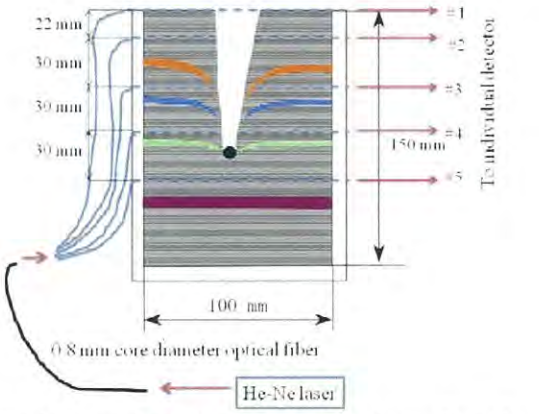

Fig. 4. Schematics of the velocity meter inside sand layer by the optical fiber breakdown.

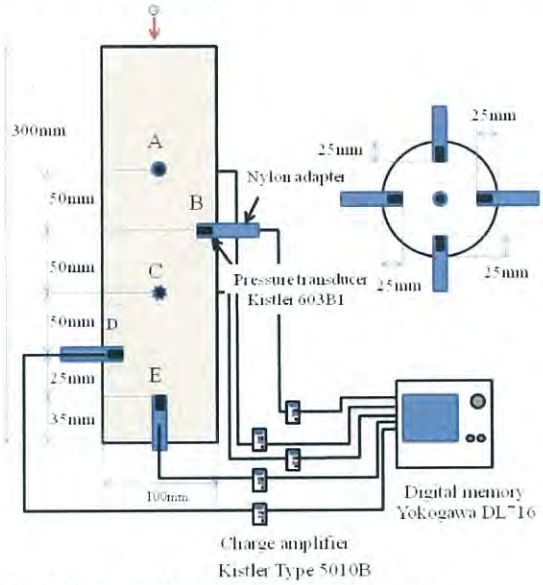

Fig. 5 Experimental setup for pressure measurement.

3. Results

3-1. Impact velocity of projectile

High-speed penetration experiments were conducted on Eglin sand and Glass beads. Parameters used for the present experiment and penetration depth were tabulated in Table. 1. All specimens were filled in test chamber with bulk density varying from 1.49 g/cm^3 to 1.58 g/cm^3 under arid conditions. Impact velocity of nine experiments varied from 1.13 to 1.26 km/s due to addition of extra powder at firing, as noted section 2.2.

Figure 6 shows relationship between penetration depth and impact velocity at bulk density of Eglin sand and Glass beads

varying from 1.55 g/cm^3 to 1.58 g/cm^3 and from 1.54 g/cm^3 to 1.55 g/cm^3, respectively. It is clear from the graph that he projectile can penetrate more deeply into Glass beads than Eglin sand at the same impact velocity. Additionally, there was negative correlation between penetration depth and impact velocity at Eglin sand under certain conditions of bulk density.

Figure 7 shows relationship between penetration depth and bulk density at impact velocity of ϕ 355~ 500μm, ϕ 500~ 710μm Eglin sand and Glass beads varying from 0.94 km/s to 1.03 km/s, from 1.25 km/s to 1.26 km/s and from 1.21 g/cm^3 to 1.27 g/cm^3, respectively.

There was negative correlation between penetration depth and bulk density at Eglin sand under certain conditions of impact velocity.

3-2. Penetration velocity of projectile inside sand layer

Figure 8 shows the output signals from fiber breakdown velocity meter. Falling edge indicates fiber breakdown.

Vertical positions of optical fibers and times of falling edge due to fiber breakdown were plotted in figure 9. Mean velocity decreased at constant acceleration rate until several tens of millimeter above the resting position.

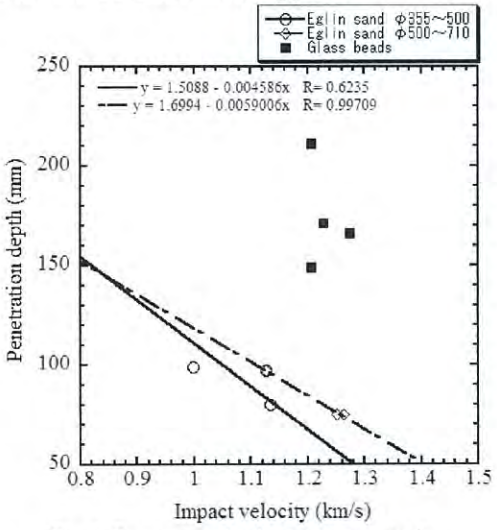

Fig. 6. Penetration depth vs. impact velocity.

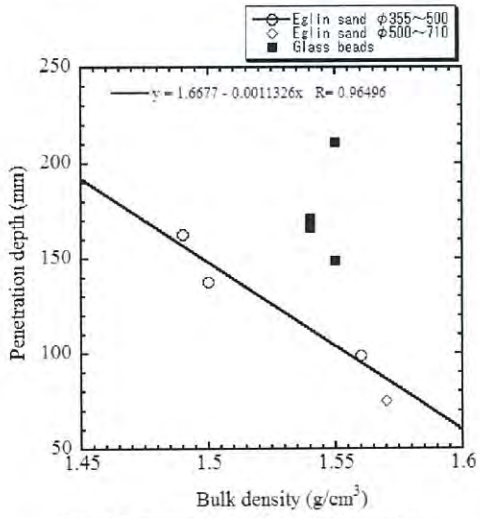

Fig. 7. Penetration depth vs. bulk density.

Table. 1 Experimental data. E: Eglin sand; G: Glass beads; a: 355~500; b: 500~710.

Shot No.	Impact velocity (km/s)	Target	Grain size (μm)	Bulk density (g/cm^3)	Penetration depth (mm)
51	1.00	E	a	1.56	99
46	1.03	E	a	1.50	138
44	0.94	E	a	1.49	163
24	1.14	E	a	1.55	80
21	1.13	E	a	1.55	97
48	0.97	E	b	1.54	209
27	1.25	E	b	1.57	75
26	1.26	E	b	1.57	75
25	1.13	E	b	1.58	97
29	1.27	G		1.54	166
28	1.23	G		1.54	171
23	1.21	G		1.55	149
22	1.21	G		1.55	211

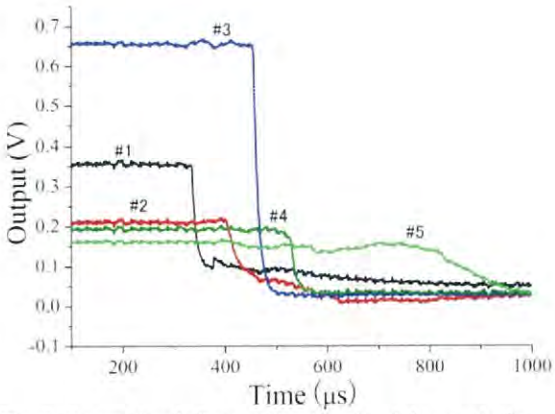

Fig. 8. Output signals from optical fiber breakdown velocity meter. Each position of optical fiber was referred to in Fig. 4.

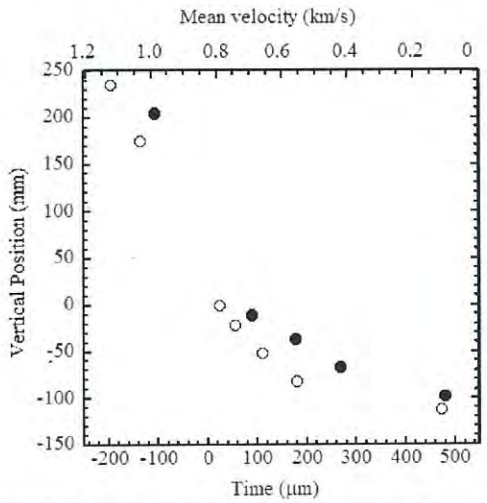

Fig. 9. Open circles indicate vertical positions of optical fibers and times of falling edge due to fiber breakdown. Closed circles indicate mean velocity. 0 mm is surface of sand layer.

3-3. Dynamic pressure inside sand layer and glass beads

The time variations of the individual pressure signals in Eglin sand are shown in Figs. 10 and 11. Impact velocity, bulk density and grain size were 1.13 km/s, 1.55 g/cm3 and 355~ 500 μm, respectively. The abscissa designates time in μs and the ordinate designates overpressures in MPa. Pressure signals in a part surrounded by a rectangular in Fig. 10 are displayed in Fig. 11. The sharp increases of signals out of individual pressure transducers clearly indicate the presence of shock waves in front of the high-speed projectile and their multiple reflection from the side wall and the expansion wave from the surface. However, since the speed of sound in this sand layer is unknown, we cannot precisely identify wave motions inside the sand layer. Hence, we have to determine the speed of sound of this specimen separately.

3-4. Deformation of sand layer

Figure 12 shows cross-section of sand layer. Crushed sand layer formed funnel shape behind stainless steel bearing, shows the penetration track of projectile. However, at the A plane, the sabot fragment following projectile penetrated and formed another small trail. As a result, more complex structure was formed than plane B. Nevertheless, it is clear that the crushed sand layer constricted in the middle. It should be considered that the decompaction and convection due to horizontal movement occurred after vertical movement behind projectile.

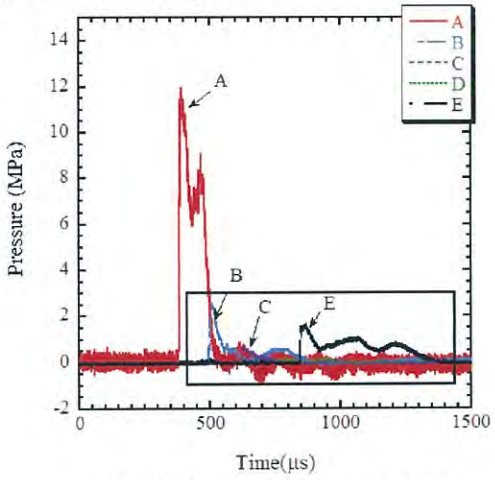

Fig. 10. Pressure signals in Eglin sand.

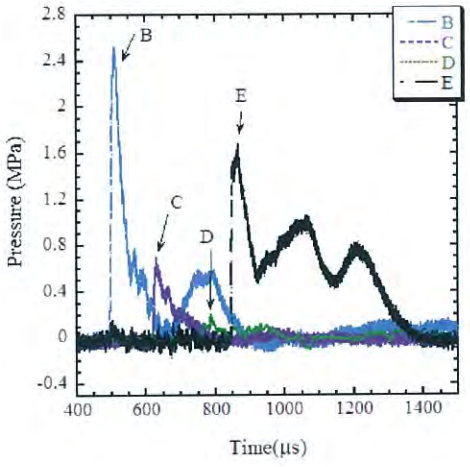

Fig. 11. Pressure signals in a part surrounded by a rectangular in Fig. 8.

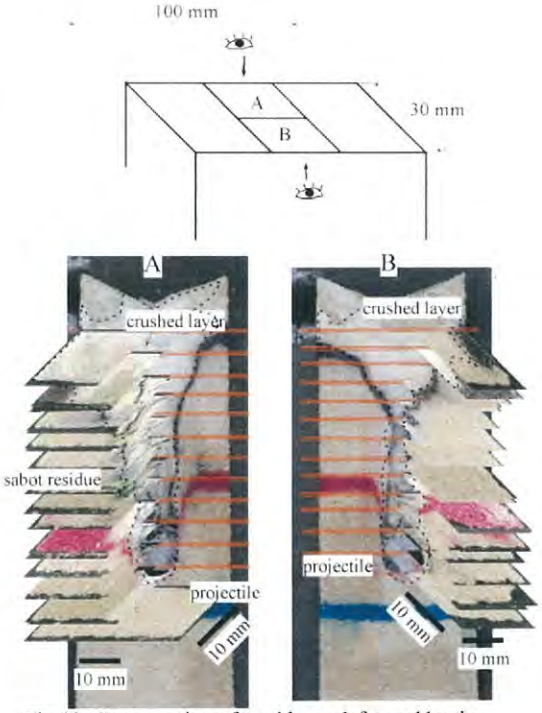

Fig.12. Cross-section of sand layer deformed by the penetration test. Grain size: 355~ 500 μm; bulk density: 1.56 g/cm^3; projectile : stainless steel bearing (3.6 grams); impact velocity : 1.00 km/s

4. Concluding remarks

Using a vertical powder gun, we launched 9.53mm diameter stainless spheres at speed ranging from 0.94 km/s to1.26 km/s into particulate media. To preserve impacted specimens, we immersed them into inorganic silicate-sealing agent and succeeded to freeze the trajectory of sphere's motion and to identify the deformation of the sand layer structure.

5. Acknowledgements

The authors wish to acknowledge to Messrs. T. Akama, M. Honna, K. Kikuta and the members of the Interdisciplinary Shock Wave research Laboratory for their devotion for performing experiments. The authors also to thank D&D Corporation for supplying the silicone sealant. This project is supported by the Grant-in-Aid for USAF.

References : (1) M. Nishida, K Tanaka, M. Okumura, Bussei Kenkyu, **88-2**, 192 (2007).